Optica Applicata, Vol. XXVIII, No. 3, 1998

Tunable axial resolution in confocal scanning microscopy by controlled symmetrical defocusing

MANUEL MARTINEZ-CORRAL, MAREK KOWALCZYK, CARLOS ZAPATA-RODRIGUEZ, PEDRO ANDRÉS

Departamento de Optica, Universidad de Valencia, 46100 Burjassot, Spain.

There is presented a quite simple technique for improving the axial resolution capacity of confocal scanning microscopes without detriment to their transverse resolution. The technique, that is based on the equal contribution to the image of the illuminating and collecting lenses, consists in symmetrical defocusing of both parts of the imaging system.

1. Introduction

Confocal scanning microscopes (CSM) are imaging systems in which the light radiated from a point source is focused onto the object by an illuminating set, then the transmitted light is imaged by a collecting set and the light, which passes through a pinhole at the center of the image plane, is detected. In this symmetrical configuration, both the illuminating and collecting sets play equal roles in the image properties. The most important feature of the CSM is their ability to form a three-dimensional (3-D) image of 3-D objects [1]. This 3-D capability results from both their high transverse resolution capacity and their optical sectioning ability. Over the last years several attempts have been made in order to achieve an improvement of the resolution capacity of the CSM either in the transverse direction [2]–[6], along the axial direction [7], [8], or simultaneously in both directions [9], [10].

The goal of this paper is to report a new technique for improving the resolution capacity of CSM in the axial direction with no detriment to resolution in transverse direction. The technique that is based on the equal contribution to the image of the illuminating and collecting lenses consists in symmetrical defocusing of both parts of the imaging system. It is also shown that the performance of the technique can even be improved by introducing a pair of axially-superresolving purely-absorbing pupil filters into both parts of the confocal setup.

2. Basic theory

Let us start with considering the transmission-mode symmetrical confocal scanning microscope depicted in Fig. 1. In this setup the plane object is illuminated with the beam focalized by the illuminating lens. If we consider that the object, whose amplitude transmittance is $t(x_0, y_0)$, is centered at the point (x_s, y_s), the amplitude

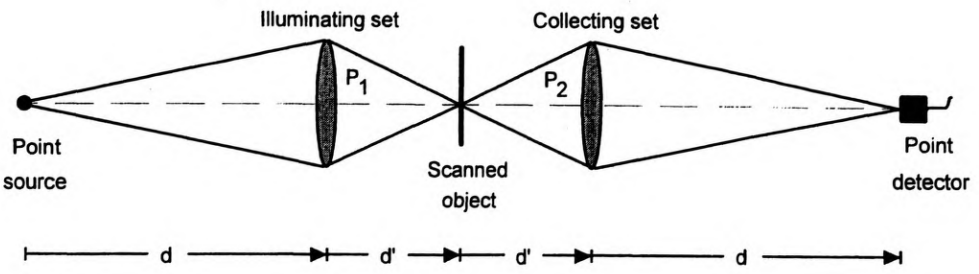

Fig. 1. Schematic layout of the transmission-mode confocal scanning microscope

distribution at the object plane can be expressed as follows:

$$U(x_0, y_0) = \exp\left[i\frac{k}{2d'}(x_0^2+y_0^2) \right] h_1(x_0, y_0) t(x_0-x_s, y_0-y_s) \tag{1}$$

where function

$$h_1(x_0, y_0) = \iint p_1(\zeta_1, \eta_1) \exp\left[-i\frac{2\pi}{\lambda d'}(\zeta_1 x_0+\eta_1 y_0) \right] d\zeta_1 d\eta_1 \tag{2}$$

is the transverse amplitude point spread function (PSF) of the illumination lens within the Fresnel approximation.

Since the function $h_1(x_0, y_0)$ falls off quite quickly, x_0 and y_0 are small enough in the exponential term of Eq. (1) to be replaced by the unity and Eq. (1) may be rewritten as

$$U(x_0, y_0) = h_1(x_0, y_0)\, t(x_0-x_s, y_0-y_s). \tag{3}$$

The amplitude distribution $U(x_0, y_0)$ is the object for the second half of the confocal system, *i.e.*, the collecting set. As $U(x_0, y_0)$ is a quite narrow function in comparison with the distance d', it can be considered, with a good approximation, that the collecting lens is in the far field region of $U(x_0, y_0)$, and then that the Fraunhofer pattern of $U(x_0, y_0)$ is at the exit pupil of this imaging system. In this case, the collecting set works as a coherent linear shift invariant (LSI) imaging formation system. Thus the amplitude distribution in the image plane can be expressed by the convolution between the geometrical image of the object and the amplitude transverse PSF of the collecting lens, that is

$$U_3(x_3, y_3; x_s, y_s) = h_1\left(\frac{x_3}{m}, \frac{y_3}{m}\right) t\left(\frac{x_3-x_s}{m}, \frac{y_3-y_s}{m}\right) \otimes \iint p_2(\zeta_2, \eta_2) \times \exp\left[-i\frac{2\pi}{\lambda d}(\zeta_2 x_3+\eta_2 y_3) \right] d\zeta_2 d\eta_2 \tag{4}$$

where m represents the lateral magnification of collecting set. If we take into account that $m = -d'/d$, Eq. (4) can be rewritten as

$$U_3(x_3,y_3;x_s,y_s) = h_1\left(\frac{x_3}{m},\frac{y_3}{m}\right) t\left(\frac{x_3-x_s}{m},\frac{y_3-y_s}{m}\right) \otimes \iint p_2(\zeta_2,\eta_2)$$
$$\times \exp\left[-i\frac{2\pi}{\lambda d'}\left(\zeta_2\frac{x_3}{-m}+\eta_2\frac{y_3}{-m}\right)\right] d\zeta_2 d\eta_2$$
$$= h_1\left(\frac{x_3}{m},\frac{y_3}{m}\right) t\left(\frac{x_3-x_s}{m},\frac{y_3-y_s}{m}\right) \otimes h_2\left(\frac{x_3}{-m},\frac{y_3}{-m}\right), \tag{5}$$

whose integral representation is

$$U_3(x_3,y_3;x_s,y_s) = \iint h_1\left(\frac{\alpha}{m},\frac{\beta}{m}\right) t\left(\frac{\alpha-x_s}{m},\frac{\beta-y_s}{m}\right) h_2\left(\frac{x_3-\alpha}{-m},\frac{y_3-\beta}{-m}\right) d\alpha d\beta. \tag{6}$$

Finally, when the point detector placed at $x_3 = y_3 = 0$ is considered we can state that the amplitude at this point is

$$U_3(0,0;x_s,y_s) \equiv U_3(x_s,y_s) = \iint h_1\left(\frac{\alpha}{m},\frac{\beta}{m}\right) t\left(\frac{\alpha-x_s}{m},\frac{\beta-y_s}{m}\right) h_2\left(\frac{\alpha}{m},\frac{\beta}{m}\right) d\alpha d\beta$$
$$= \iint h_1(\alpha,\beta)\, t(\alpha-x_s,\beta-y_s)\, h_2(\alpha,\beta) d\alpha d\beta$$
$$= [h_1(x_s,y_s)\, h_2(x_s,y_s)] \otimes t(x_s,y_s). \tag{7}$$

Based on the comparison of Eq. (7) with the equation that provides the amplitude distribution in the image plane for a coherent LSI imaging formation system we can state that, from an analytical point of view, a transmission mode CSM behaves as a coherent imaging system with an effective amplitude transverse PSF that is given, precisely, by the product of the two independent amplitude PSFs of illuminating and collecting sets.

As we are interested in radially-symmetric confocal scanning systems we particularize here, and in all the study developed below, our equations for the case of two radially-symmetric pupil functions with the same radial extent. In this case, the intensity PSF of the CSM is

$$I(v) = |h_1(v)h_2(v)|^2 = \left|2\int_0^1 p_1(\rho)J_0(v\rho)\rho d\rho\right|^2 \left|2\int_0^1 p_2(\rho)J_0(v\rho)\rho d\rho\right|^2 \tag{8}$$

where $\rho = r/r_m$ represents the normalized radial coordinate at the pupil plane, and $v = r_m r_0/\lambda d'$ stands for the radial variation in the object plane, r_m being the maximum radial extent of the pupil.

The function $I(v)$ in Equation (8), which stands for the transverse intensity PSF of the confocal scanning imaging system, is not a transverse PSF in the conventional way, because it does not represent the intensity distribution in the image plane for a point object. On the contrary, it represents the function that can be composed of the values of the intensity collected by the point detector when a pinhole is scanned through the confocal plane.

As the main feature of CSM is its ability to form three-dimensional images, it is convenient to extend the concept of intensity PSF up to three dimensions. In this sense it is easy to show that the intensity achieved at the point detector when a pinhole is centered at a normalized distance (v, u) from the confocal point is given by

$$I(v,u) = |h_1(v,u)h_2(v,-u)|^2 \tag{9}$$

where

$$h(v,u) = 2\int_0^1 p(\rho)\exp\left(-i\frac{1}{2}u\rho^2\right)J_0(v\rho)\rho\,\mathrm{d}\rho \tag{10}$$

stands for the 3-D amplitude PSF of illuminating (or collecting) lens, being

$$u = \frac{2\pi r_m^2 z}{\lambda d'(d'+z)}, \tag{11}$$

u denotes the axial coordinate in optical units, where z represents the axial distance as measured from the confocal point.

If we particularize now Equation (9) for axial points, $v = 0$, we arrive at the axial intensity PSF of the system given by

$$I(0,u) = |h_1(0,u)h_2(0,-u)|^2, \tag{12}$$

where

$$h(0,u) = 2\int_0^1 p(\rho)\exp\left(-i\frac{1}{2}u\rho^2\right)\rho\,\mathrm{d}\rho. \tag{13}$$

In the above equation, an irrelevant premultiplying factor has been omitted. In order to analyze the axial behaviour of CSM, it is convenient to perform the next geometrical mapping

$$\zeta = \rho^2 - 0.5, \qquad q_j(\zeta) = p_j(\rho), \qquad j = 1,\ 2, \tag{14}$$

which allows us to convert Eq. (13) into a 1-D Fourier transform of the mapped version of $p(\rho)$, *i.e.*,

$$h(0,u) = \int_{-0.5}^{0.5} q(\zeta)\exp\left(-i\frac{1}{2}u\zeta\right)\mathrm{d}\zeta. \tag{15}$$

The function defined in Eq. (12) is designed with the values of intensity collected by the point detector when a pinhole is canned through the optical axis, and constitutes an important figure of merit for evaluating the axial resolution capacity of CSMs.

Up to now, we have described the formulation corresponding to CSM working in transmission mode, see Fig. 1. However, other alternative geometry in CSM is that

corresponding to the reflection mode (see Fig. 2). When calculating different PSFs in such a case we have to take into account two facts. First, in reflection mode the same lens works as illuminating and collecting lens, hence $p_1(\rho) = p_2(\rho) = p(\rho)$. Second, in reflection mode the object for the collecting set is the reflected image of $h_1(v,u)$. Taking account of these facts, the 3-D intensity PSF of a radially-symmetric reflection CSM can be written as follows:

$$I(v,u) = |h(v,u)|^4. \tag{16}$$

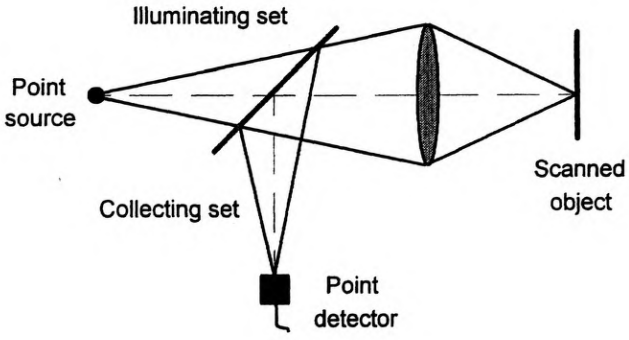

Fig. 2. Schematic layout of the reflection-mode confocal scanning microscope

The major motivation for confocal microscopy is the optical sectioning, or depth discrimination. The axial intensity PSF presented in Eq. (12) gives a measure of the depth discrimination for the objects whose main features are points. However, when the main object features are some others it is necessary to define other functions for evaluating the optical sectioning. In this sense, the use of the so-called *integrated intensity function* is appropriate. It is defined as

$$I_{\text{int}}(u) = 2\pi \int_0^\infty I(v,u) v \, dv. \tag{17}$$

This function evaluates the power in the detected image corresponding to variable axial positions of the object, and give us information on how the microscope discriminates between different parts of the object which are out of the confocal plane.

In the case of objects, whose main features are planes, the responses are evaluated in terms of the so-called z-function. This function, defined only for CSMs working in the reflection mode, is obtained by evaluating the intensity detected when a perfect planar reflector (PPR), which is placed perpendicularly to the optical axis of the device, is axially scanned through the focus (see Fig. 3). For calculation of the function, z, which will be denoted here as $I(u)$, it has to be considered that for a given axial position u_0 of the PPR the amplitude distribution generated by the illuminating system over the confocal plane, *i.e.*, the amplitude distribution that is imaged by the collecting system, we have $h(v, 2u_0)$. So the amplitude distribution at the detector plane is

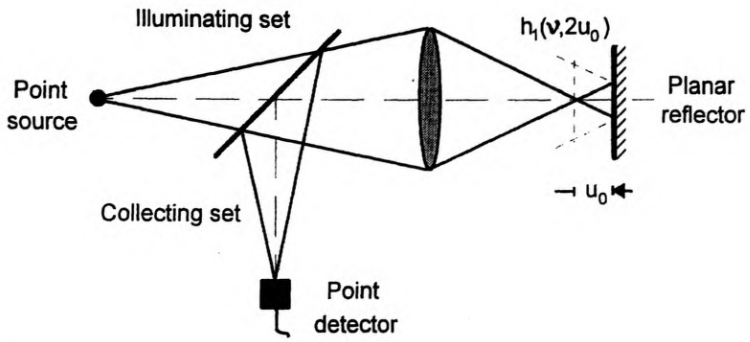

Fig. 3. PPR placed at the axial coordinate u_0 provides an amplitude $h_1(v, 2u_0)$ over the confocal plane

$$U_3(v;u_0) = h(v,2u_0) \otimes h(v,0). \tag{18}$$

Particularizing now Eq. (18) for the axial point detector $v = 0$, we obtain

$$U_3(0;u_0) = \int_0^\infty h(v,2u_0)\,h(v,0)v\mathrm{d}v. \tag{19}$$

If we take into account the power theorem [11] that states that the area of the product of two functions is equal to the area of the product of their spectra, Eq. (19) can be rewritten, apart from a constant factor, as

$$U_3(0;u_0) = \int_0^1 p(\rho)\exp\left(-i\frac{1}{2}2u_0\rho^2\right)p(\rho)\rho\mathrm{d}\rho = \int_{-0.5}^{0.5}[q(\zeta)]^2\exp(-iu_0\zeta)\mathrm{d}\zeta \tag{20}$$

where the geometrical mapping defined in Eq. (14) has been introduced. Finally, the squared modulus of Eq. (19) provides the formula for the function z

$$V(z) = I(u) \equiv |U_3(0;u)|^2 = \left|\int_{-0.5}^{0.5}[q(\zeta)]^2\exp(-iu\zeta)\mathrm{d}\zeta\right|^2. \tag{21}$$

This formula indicates that when a PPR is axially scanned through the confocal volume of a reflection mode CSM, the detected intensity is given simply by the 1-D Fourier transform of the square of the mapped version of the amplitude transmittance of the pupil.

3. Symmetrical defocusing

In order to increase the axial resolution capacity of CSMs, there is proposed a quite simple technique consisting in introducing a slight symmetrical defocusing in both parts, illuminating and collecting, of the confocal setup. From a practical point of view, the symmetrical defocusing in the setup can be introduced either by a slight axial mispositioning of the collecting set with respect to the illuminating one, or

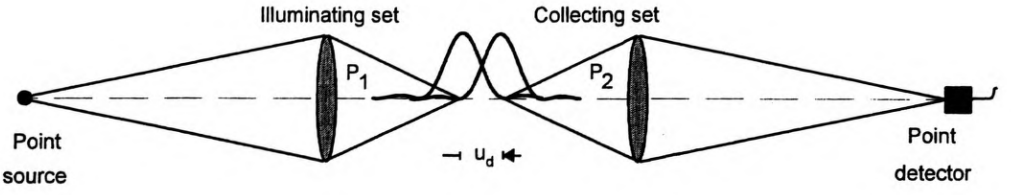

Fig. 4. Schematic layout of the transmission-mode disadjusted confocal scanning microscope

simply by a slight symmetrical axial displacement of both the point source and the point detector. In both cases, the displacement implicates that the point which focalizes the illuminating beam does not coincide with the point whose image due to the collecting lens is in the point detector (see Fig. 4). From the mathematical point of view the symmetrical defocusing implicates that the effective pupil functions are

$$p'_j(\rho) = p_j(\rho)\exp\left(-i\frac{1}{2}\frac{u_d}{2}\rho^2\right), \qquad j = 1,\ 2 \tag{22}$$

where the parameter u_d represents the axial displacement between both parts of the setup, and can be positive or negative.

Now, the axial intensity PSF is given by the squared modulus of the product of two independent amplitudes PSF that are relatively displaced along an axial distance u_d, that is

$$I(0,u) = |h'_1(0,u)h'_2(0,-u)|^2 \tag{23}$$

where

$$h'_1(0,u) = 2\int_0^1 p_1(\rho)\exp\left[-i\frac{1}{2}\left(u+\frac{u_d}{2}\right)\rho^2\right]\rho\,\mathrm{d}\rho$$

$$= \int_{-0.5}^{0.5} q_1(\zeta)\exp\left[-i\frac{1}{2}\left(u+\frac{u_d}{2}\right)\zeta\right]\mathrm{d}\zeta \tag{24}$$

and

$$h'_2(0,-u) = 2\int_0^1 p_2(\rho)\exp\left[i\frac{1}{2}\left(u-\frac{u_d}{2}\right)\rho^2\right]\rho\,\mathrm{d}\rho$$

$$= \int_{-0.5}^{0.5} q_2(\zeta)\exp\left[i\frac{1}{2}\left(u-\frac{u_d}{2}\right)\zeta\right]\mathrm{d}\zeta. \tag{25}$$

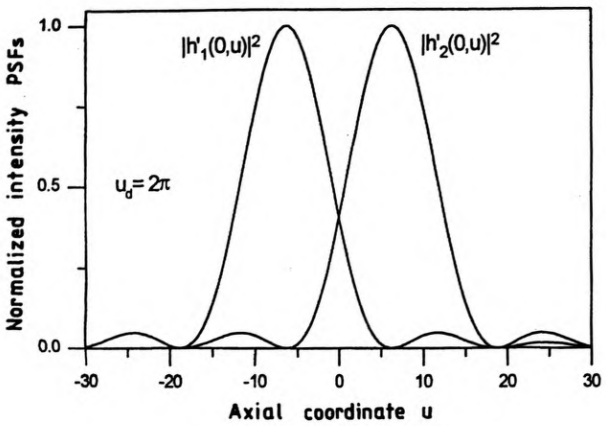

Fig. 5. Normalized axial intensity PSFs for displaced illuminating and collecting setups

In the case of two clear circular pupils, the mapped functions are $q_1(\zeta) = q_2(\zeta) = 1$, and then the axial intensity PSF of the CSM is given by the product of two sine functions but separated by an axial distance u_d (see Fig. 5). When the product is performed, it is obtained an axial intensity PSF in which the width of the central lobe is given by the distance between the first zero "at the right" of $h'_1(0,u)$ and the first zero "at the left" of $h'_2(0,-u)$. Then the magnitude of the narrowing generated, in comparison with the width of the central lobe for the non-disadjusted case, is precisely equal to u_d. It is clear that simply by a continuous variation of u_d, *i.e.*, by gradual axial mispositioning of collecting set, we are able to control at will the width of the axial intensity PSF, and then to obtain tunable axial superresolution in confocal scanning microscopy. For illustrating this effect, in Fig. 6 we have plotted

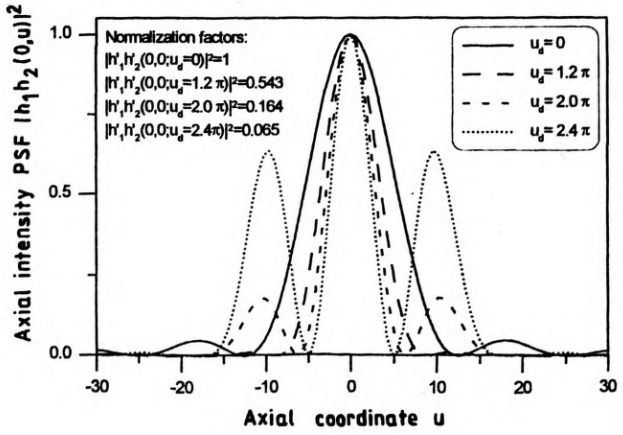

Fig. 6. Normalized axial intensity PSF for disadjusted scanning confocal microscopes with variable values of disadjusted parameters

the axial intensity PSF for some values of disadjusted parameter u_d, including the non-disadjusted case $u_d = 0$. The plots obtained prove that as the value of disadjusted parameter u_d increases the central lobe of the normalized axial intensity PSF gradually decreases.

It should be pointed out that behind the narrowness of the central lobe of PSF, two collateral effects appear. On the one hand, the amount of energy collected by the point detector in this case is much lower than in the non-disadjusted case. However, due to the special nature of confocal scanning microscopes, this loss of energy has no essential importance because in such systems the source of power can arbitrarily be modified, within certain limits, of course. The second collateral effect is a substantial increase in the strength of the secondary lobes. This limits, in practice, the maximum value of u_d that can be used. From Fig. 6 it is apparent that for the values of u_d lower than 2π the relative strength of lateral lobes is still admissible, while for $u_d > 2\pi$ the strength fast increases as u_d increases. This fact implies that, in practical terms, our method permits the reduction of the width of the central lobe up to a factor 1/2.

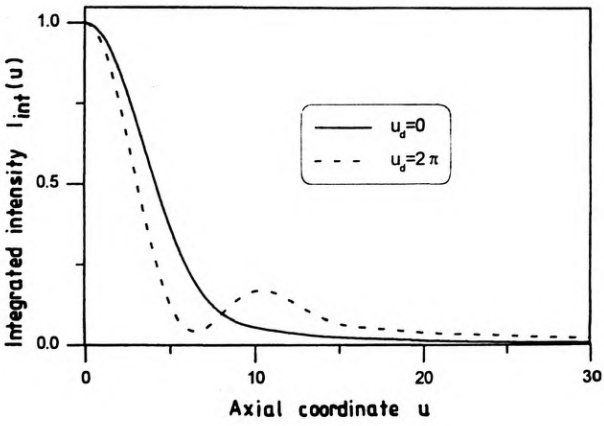

Fig. 7. Integrated intensity function for confocal and disadjusted system

As for the behaviour of the integrated intensity parameter, in Fig. 7 we have depicted the function $I_{\text{int}}(u)$ representing the disadjusted parameter value $u_d = 2\pi$ in comparison to the non-disadjusted parameter value. It is apparent from this figure that the curve corresponding to the disadjusted setup falls off much faster. Consequently, the proposed method provides an important improvement in the capacity of discrimination between different parts of the object which is not in the confocal plane.

With regard to the function $V(z)$, it is easy to show that the symmetrical defocusing does not affect its value. Then it is concluded that the proposed method provides no changes in the axial resolution for objects whose main features are planes.

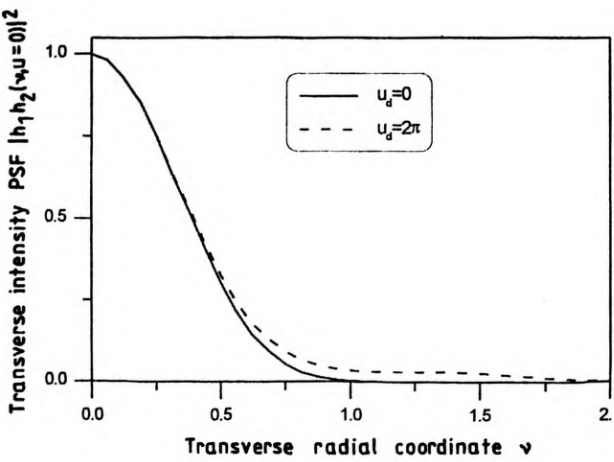

Fig. 8. Transverse behaviour of symmetrically-defocused system in comparison with confocal one

Finally, we would like to emphasize that due to the hellyptical nature of 3-D intensity PSF of a lens there are not found crucial differences between its transverse PSF in the focal plane and a slightly defocused plane. Consequently, when the product of displaced PSFs is carried out, a transverse intensity PSF is obtained for the CSM whose slope in the confocal plane is quite similar to that obtained in the corresponding non-disadjusted setup, as it is shown in Fig. 8, where we have compared the cases $u_d = 2\pi$ and $u_d = 0$. Then, it is concluded that our method practically does not affect the resolution of the device in the transverse direction. This fact allows us to recognize that symmetrical defocusing permits obtaining a 3-D intensity PSF in which the area covered with the central lobe can gradually be reduced. Thus, in this sense, it can be stated that the method permits us to improve the 3-D resolution in CSM or, equivalently, that it provides a 3-D superresolution effect.

4. Use of superresolving pupil filters

As it is pointed out in previous section, the proposed method is based on the fact that the width of the central lobe of axial intensity PSF for disadjusted system is that of the adjusted one minus the value of disadjusted parameter u_d. Thus, it is clear that if we deal with confocal system with axial PSF that has been narrowed by other methods, a higher axial superresolving effect can be achieved when the symmetrical defocusing is introduced.

On the basis of this fact we propose to combine the symmetrical defocusing with the use, in both parts of confocal system, of purely-absorbing axially-superresolving pupil filters. Since a practical implementation of continuously varying pupil filters is not an easy task [12], [13], the filter we propose to exemplification of the method is one of the family of axially-superresolving filters composed of two annuli of equal areas [8] whose mapped amplitude transmittance can be expressed as

$$q(\zeta) = \mathrm{rect}(\zeta) - \mathrm{rect}(\zeta/\mu) \quad \text{with } \mu = 1/3, \tag{26}$$

and whose 2-D actual form is represented in Fig. 9.

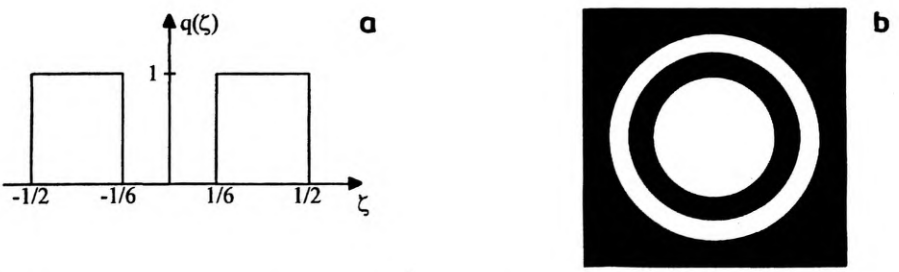

Fig. 9. Member of the family of axially superresolving pupil filters: **a** — mapped function $q(\zeta)$, **b** — actual 2-D representation

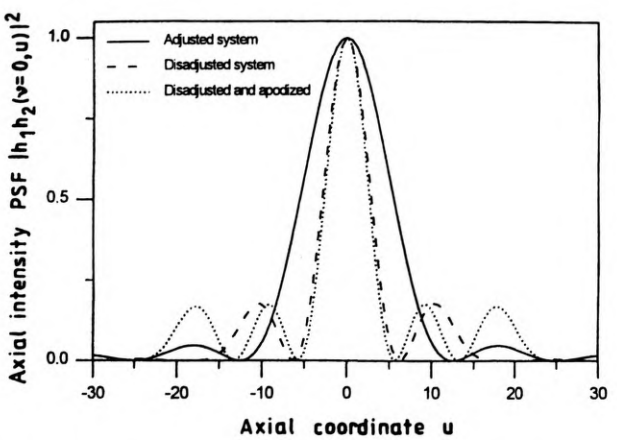

Fig. 10. Integrated intensity function for confocal, disadjusted, and disadjusted and apodized systems

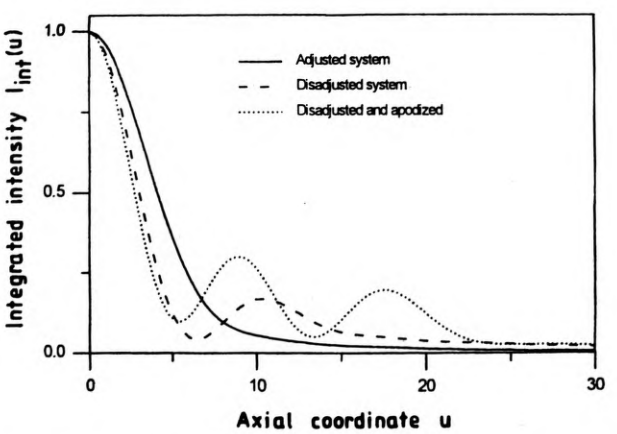

Fig. 11. Integrated intensity for the three setups under study

In Figure 10, it is shown the axial intensity PSF for an apodized and disadjusted ($u_d = 2\pi$) confocal system in comparison with those corresponding to nonapodized systems. This figure illustrates the fact that the axial resolution can be improved by introducing a pair of axially superresolving masks. In Figure 11, we have plotted the integrated intensity for the three geometries described above. This figure corroborates the proper combination of apodization and symmetrical defocusing increments in the sectioning capacity of confocal systems.

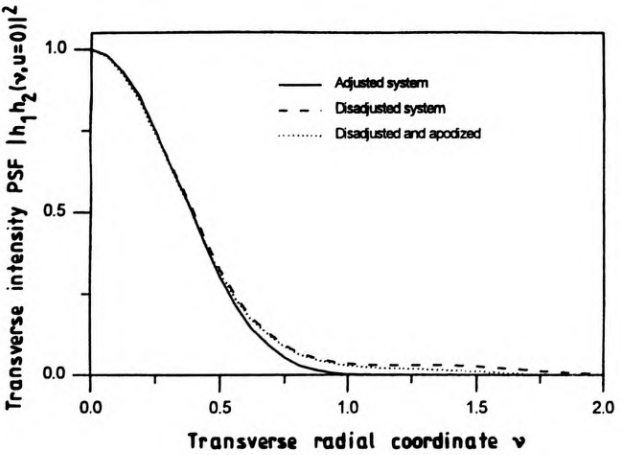

Fig. 12. Transverse behaviour for the three setups under study

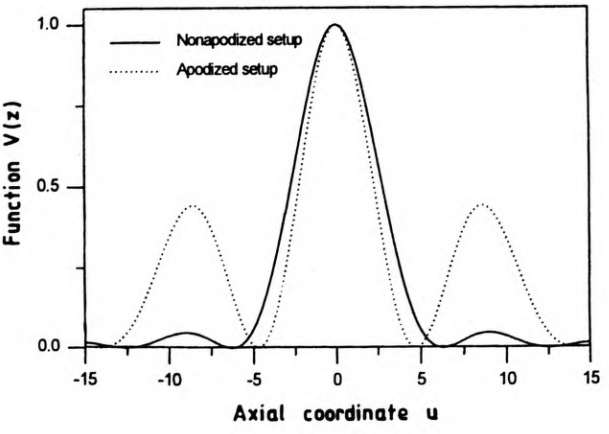

Fig. 13. Central lobe of the function $V(z)$ suffers a narrowing when apodizers are used

In Figure 12, it is depicted the transverse intensity PSFs for the three described setups. This figure indicates that the introduction of proposed filters does not affect the transversal resolution of the confocal system. Finally, in Fig. 13 we present the

function $V(z)$ for apodized and nonapodized setups. From this figure it is clear that the most important feature of combining symmetrical defocusing with apodization is a significant reduction in the dimensions of the central lobe of the function $V(z)$, and consequently a noticeable increase in the capacity of discrimination between different planes in the reflection mode.

5. Conclusions

We have presented a quite simple method for tuning at will the axial resolution of confocal scanning imaging systems. The method simply consists in a controlled axial disadjustment of both parts of the confocal setup. It is also demonstrated that the method does not affect the transverse resolution of the system, providing an effective 3-D superresolution effect. The performance of the system can even be improved by combining the symmetrical defocusing with a proper use of axially-superresolving pupil filters.

Acknowledgments – This work was supported by the Dirección General de Investigación Científica y Técnica (grant PB93-0354-CO2-01), Ministerio de Educación y Ciencia, Spain. C. J. Zapata-Rodríguez gretefully acknowledges financial support from this institution.

References

[1] WILSON T., [Ed.] *Confocal Microscopy*, Academic, London 1990.
[2] HEGEDUS Z. S., Opt. Acta **32** (1985), 815.
[3] HEGEDUS Z. S., SARAFIS V., J. Opt. Soc. Am. A **3** (1986), 1892.
[4] GROCHMALICKI J., PIKE E. R., WALKER J. G., BERTERO M., BOCCACCI P., DAVIES R. E., J. Opt. Soc. Am. A **10** (1993), 1074.
[5] WALKER J. G., PIKE E. R., DAVIES R. E., YOUNG M. R., BRAKENHOFF G. J., BERTERO M., J. Opt. Soc. Am. A **10** (1993), 59.
[6] WILSON T., HEWLETT S. J., J. Modern Opt. **37** (1990), 2025.
[7] SHEPPARD C. J. R., GU M., Optics Commun. **84** (1991), 7.
[8] MARTÍNEZ-CORRAL M., ANDRÉS P., OJEDA-CASTAÑEDA J., SAAVEDRA G., Opt. Commun. **119** (1995), 491.
[9] MARTÍNEZ-CORRAL M., ANDRÉS P., SILVESTRE E., BARREIRO J. C., Proc. SPIE **2730** (1995), 634.
[10] DING Z., WANG G., GU M., WANG Z., FAN A., Appl. Opt. **36** (1997), 360.
[11] BRACEWELL R. N., *The Fourier Transform and its Applications*, Chapt. 6, McGraw-Hill, 1978.
[12] WEISSBACH S., WYROWSKI F., Appl. Opt. **31** (1992), 2518.
[13] KOWALCZYK M., MARTÍNEZ-CORRAL M., CICHOCKI T., ANDRÉS P., Opt. Commun. **114** (1995), 211.

Received July 22, 1998